

Characterization of chicken manure biochar relevant to its potential use in remediation of Cd contaminated water

Cuixia Yan^{a,b}, Tao Sun^{a,b}, Hongtao Jia^b, Yingming Xu^a, Yuebing Sun^{a,*}

^aKey Laboratory of Original Environmental Pollution Prevention and Control, Ministry of Agriculture and Rural Affairs (MARA)/ Tianjin Key Laboratory of Agro-Environment and Agro-Product Safety, Agro-Environmental Protection Institute, (MARA), Tianjin 300191, China, Tel. +86-22-23618061; Fax: +86-22-23618060; emails: sunyuebing@aepi.org.cn (Y.B. Sun), 905358926@qq.com (C.X. Yan), stao1211@163.com (T. Sun), ymxu1999@126.com (Y.M. Xu)

^bCollege of Grassland and Environment Sciences, Xinjiang Key Laboratory of Soil and Plant Ecological Processes, Xinjiang Agricultural University, Urumqi 830052, China, email: jiahongtao2015@126.com (H.T. Jia)

Received 7 June 2020; Accepted 8 January 2021

ABSTRACT

Biochars derived from chicken manure were prepared by anaerobic pyrolysis at 200°C, 400°C, 600°C, and 800°C (referred as CBC200, CBC400, CBC600 and CBC800, respectively). The results indicated chicken manure biochars (CBC) prepared at higher temperatures exhibited higher aromaticity. The kinetics and isothermal equilibria of Cd(II) adsorption onto CBC were well fitted using the pseudo-second-order kinetic model and Langmuir model. The adsorption process was able to achieve equilibrium at 720 min and the maximum Cd(II) adsorption capacities of CBC produced at 200°C–800°C were 45.50–52.02 mg g⁻¹. The spectroscopic surface chemistry analyses using scanning electron microscopy with transmission electron microscopy, Fourier-transform infrared spectroscopy, ¹³C nuclear magnetic resonance and Raman spectra indicated that the adsorption mechanism consisted of pore filling, complexation, precipitation and C- π interaction. Therefore, CBC could employ as an effective agent for the remediation of Cd contaminated water.

Keywords: Chicken manure; Pyrolysis temperature; Cd; Adsorption; Interaction mechanism

1. Introduction

Cd is released into the environment through anthropogenic activities, such as mining and metal ore processing [1]. Eventually harming human health after prolonged exposure, by conditions such as hypertension, anemia, and bone and kidney damage [2]. Therefore, the removal of Cd from wastewater is essential and urgent. Currently established technologies for the removal of potentially toxic metals from wastewater include adsorption, chemical precipitation, electro-coagulation, coagulation–

flocculation, ion-exchange, membrane filtration, packed-bed filtration, flotation, and electrochemical processing [3].

Research attention has primarily focused on effective environmental protectants in the form of widely applicable adsorption materials for the removal of potentially toxic metals from water. Biomass (sludge, poultry manure, crop residues, etc.), a renewable energy source, can be pyrolyzed into biochar (BC) as an environmental-friendly function material [4]. BC is a solid form of black carbon obtained by the anoxic or aerobic pyrolysis of biomass; its characteristics include porosity, oxygen-containing

* Corresponding author.

and aromatic functional groups, high surface area relative to mass, high pH, and cation exchange capacity [5,6]. BC is a passivation material and has demonstrated potential as a highly efficient, low-cost adsorbent used in the removal of potentially toxic metals from soil or sewage [7]. Experts have recently extensively researched the environmental and agricultural applications of BC [8]. The adsorption mechanisms of potentially toxic metals by BC are strongly affected by the raw materials, pyrolysis time, and especially the pyrolysis temperature [9]. Researchers studying the Cr(VI) adsorption mechanism of ramie residue-based BC pyrolyzed at different temperatures found that aromatic structures contributed to adsorption by higher-temperature BCs, while carboxyl and hydroxyl groups dominated adsorption by lower-temperature BCs [10]. Jiang and Xu [11] found that the elemental contents, surface areas, and porosities of BCs are significantly affected by pyrolysis temperatures. These factors affect their capacities to adsorb potentially toxic metals. Therefore, research on the potentially toxic metals adsorption capacities of BCs produced at different pyrolysis temperatures and times is very important in developing methods for treating sewage [12]. The objectives of the study were to investigate: (1) the characteristics of sorption kinetics and isotherm of Cd onto chicken manure biochar (CBC); (2) the mechanisms of Cd adsorption using scanning electron microscopy with transmission electron microscopy (SEM-TEM), Fourier-transform infrared spectroscopy (FTIR), Raman spectroscopy, and ^{13}C solid-state nuclear magnetic resonance (^{13}C -NMR).

2. Materials and methods

Chicken manure was collected and pyrolyzed at 200°C, 400°C, 600°C, and 800°C for 2 h in an N_2 atmosphere, which was referred as CBC200, CBC400, CBC600, and CBC800, respectively. The adsorption kinetics studies were conducted in 1 L beakers by mixing 4.00 g of CBC with 1,000 mL 200 mol L^{-1} Cd(II) (containing 0.01 mol L^{-1} NaNO_3). The initial pH of the Cd(II) solutions was adjusted to 5.0 using 0.1 mol L^{-1} HNO_3 or 0.1 mol L^{-1} NaOH. The beakers were shaken by a magnetic mixer at 200 rpm and 298 K for 24 h. Samples were taken at 0, 3, 5, 7, 10, 15, 30, 60, 120, 240, 480, and 1,440 min. After sampling, the sample solutions were filtered using 10 mL syringes and 0.45 μm membrane filters to obtain solution supernatants. The concentration of Cd(II) was analyzed by inductively coupled plasma mass spectrometry (ICP-MS) (iCAP Q, Thermo Scientific, USA) and the pH value of the solution was determined. To study the adsorption isotherms, 25 mL of Cd(II) solution, containing 0.01 mol L^{-1} NaNO_3 , and 0.1 g of CBC were blended in 50 mL polypropylene tubes. The 0.1 mol L^{-1} HNO_3 or NaOH were used to adjust the Cd(II) solution concentrations to 5, 10, 15, 25, 50, 80, 100, 150, and 200 mg L^{-1} . These were mixed in a thermostatic reciprocating shaker (200 rpm at temperatures of 288, 298, and 308 K) for 12 h. The supernatant of Cd(II) was collected and analyzed by ICP-MS.

The microstructural morphologies of the CBCs before and after adsorption were characterized by SEM-TEM (SU3500 JEM-2010, Japan), FTIR spectra (Bruker Tensor, Germany) and cross-polarization-magic angle spinning

(CP-MAS) ^{13}C nuclear magnetic resonance (^{13}C -NMR) spectra (JNM-ECZ 600R, Japan).

3. Results and discussion

3.1. Characterization of CBC

The microstructural morphologies of the CBCs, as characterized by SEM-TEM, are shown in Fig. 1. The scanning electron microscopy (SEM) images of the CBCs illustrated their morphological and structural changes like the increase of pyrolysis temperatures (Fig. 1a–d). Surface pore morphologies of the CBCs were obtained from the direct pyrolysis of the chicken manure material, whereas the longitudinal section of CBCs has a rough surface which promotes a large area of contact to perform the adsorption process of Cd(II) [13]. A comparative analysis showed that the pore structures of the CBC were developed with the increase of pyrolysis temperature. This may be attributed to the organic matter decomposition of the biochar [14]. The decomposition of protein and fats at higher pyrolysis temperatures resulted in the increase of the porosity and specific surface area of CBCs [12]. The transmission electron microscopy (TEM) micrographs in Fig. 1A–D show smooth and neat edges in the CBCs before Cd(II) adsorption. These show good agreement with the morphologies presented in the SEM images. The CBC800 sample shows a transparent film located at the edge.

The surface functional groups of the CBCs using the FTIR spectra are shown in Fig. 2. The spectra displayed several adsorption peaks within the range 500–4,000 cm^{-1} . Before Cd(II) adsorption, the significant absorption peaks at 3,310; 1,430 and 1,032 cm^{-1} may correspond to the stretching vibrations of $-\text{OH}$, $\text{C}=\text{O}$, and $\text{Si}-\text{O}-\text{Si}$ groups, respectively [15]. The absorption peaks at 2,840–2,924 cm^{-1} may indicate the vibrations of methyl ($-\text{CH}$) and methylene ($-\text{CH}_2$) groups [16]. The $-\text{OH}$ and $-\text{CH}_2$ peaks may disappear in the spectra from CBC600 and CBC800 because the increased pyrolysis temperatures may enhance the decomposition of organic compounds, yielding fewer hydroxyl and alkane groups in the CBCs, this may result from decarbonylation, decarboxylation and dehydration reactions [14]. The absorption peaks at 876 cm^{-1} in the CBC spectra were attributed to $\text{C}-\text{O}-\text{C}$ stretching vibrations and symmetric stretching vibrations of cellulose and hemicellulose [17].

Fig. 3a shows the ^{13}C -NMR spectra of the CBCs. The spectra of CBC200 and CBC400 are very similar in Fig. 3a, while it varied greatly for CBC600 and CBC800. The methoxy groups $-\text{OCH}_3$ are identified by the peak at 50–65 ppm [18,19]. Whereas 30–45 ppm is designated to the α and β carbons in the methylene groups [20]. The peaks of CBC200 and CBC400 were mainly distributed in the alkyl carbon at 0–90 ppm and the peaks of CBC600 and CBC800 were mainly distributed in aromatic carbon regions at 90–160 ppm, showing that pyrolysis temperatures of <400°C were insufficient for complete pyrolysis and aromatic carbon becomes the main component in CBCs pyrolyzed at temperatures >800°C [21]. The peak near 173 ppm was traditionally assigned to carboxyl groups. With increasing pyrolysis temperature, the aliphatic compounds (alkyl carbon), carbohydrates (methoxy carbon, hydroxyl carbon),

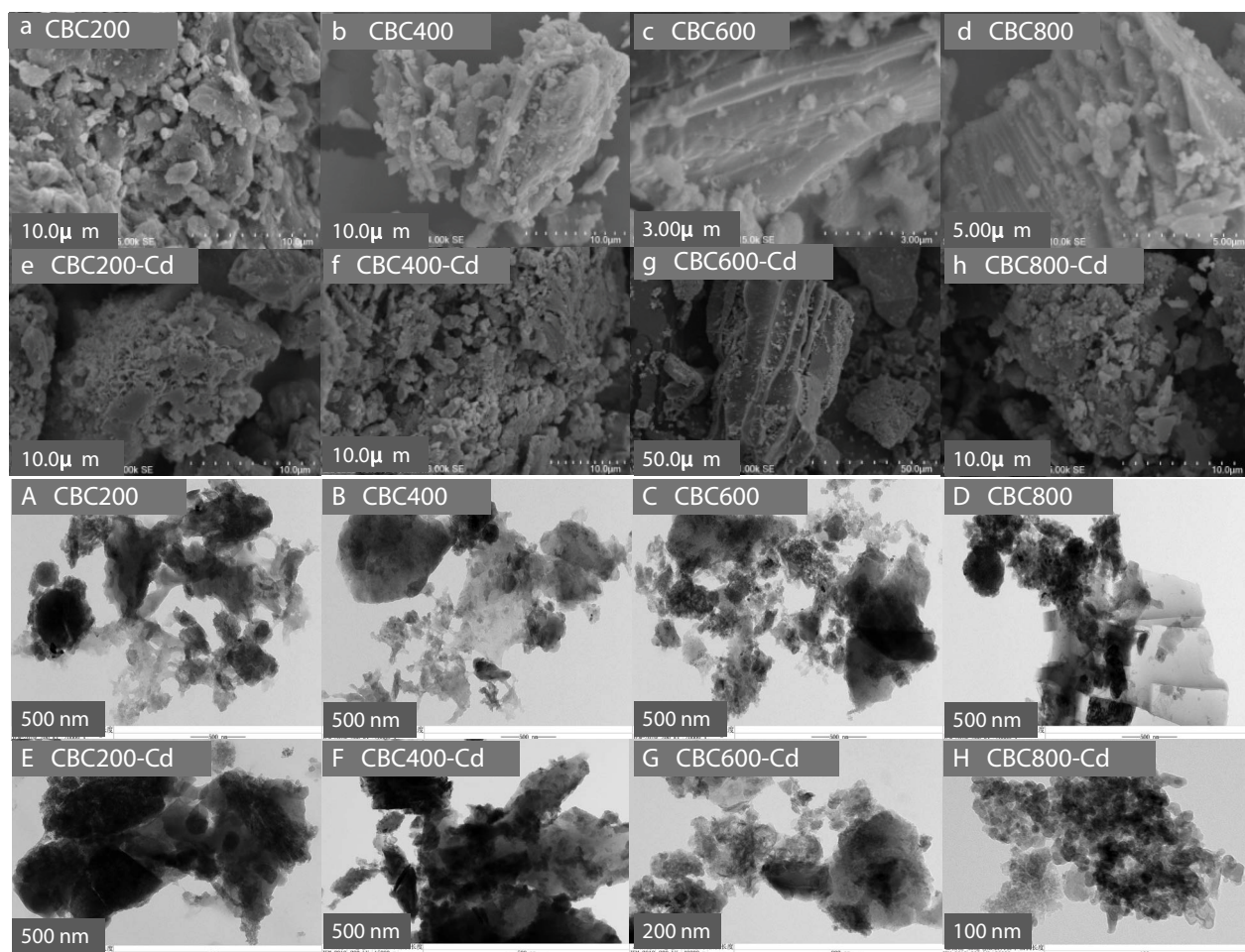


Fig. 1. Scanning electron microscope (SEM) and transmission electron microscopy (TEM) images of chicken-manure biochars (CBCs). Note: (a–d) and (e–h) refer before and after Cd(II) adsorption using SEM, and (A–D) and (E–H) refer before and after Cd(II) adsorption using TEM. The numbers in the image labels indicate the CBC pyrolysis temperatures.

carboxyl carbons, and carbonyl carbons were converted increasingly to aromatic carbons.

Structural variations observed by Raman spectroscopy of CBCs obtained at four different pyrolysis temperatures are shown in Fig. 4. The Raman spectra showed the broad bands of CBC600 and CBC800 at approximately 1,350 and 1,593 cm^{-1} which represented D band related to disordered graphene layer edges and G band related to an ideal graphitic lattice, respectively [22]. The D band and G band was not observed in the spectra from CBC200 and CBC400, indicated that the aromatization degree of CBC prepared at low temperature is relatively low [23]. The intensity ratio of the D band and G band (I_D/I_G) defined the degree of disorder in the biochar. The I_D/I_G ratio of CBC600 and CBC800 were 3.23 and 3.72, respectively, indicating that the aromaticity of biochar increases with the increase of pyrolysis temperature [24].

3.2. Kinetic of Cd adsorption

The kinetics of Cd(II) adsorption by the four chicken manure BCs can be well described by pseudo-first-order and pseudo-second-order models. The linear regression constants

(R^2) were typically used to determine the best-fitting kinetic models. The adsorption capacity of Cd(II) is given as:

$$Q_e = \frac{(C_0 - C_e)V}{m} \quad (1)$$

where Q_e (mg g^{-1}) is the adsorption capacity of Cd(II) ions. C_0 and C_e (mg L^{-1}) are the initial and equilibrium concentrations of Cd(II) ions in solution, respectively. V (L) is the volume of the Cd(II) solution, and m (g) is the mass of CBC.

The actual performance of CBC was also evaluated using the partition coefficient (P_c), which was calculated using the following equation [25]:

$$P_c = \frac{Q_e}{C_e} \quad (2)$$

The unit of P_c is $\text{mg g}^{-1} \mu\text{M}^{-1}$.

The pseudo-first-order model equation is as follows:

$$Q_t = Q_e (1 - e^{-kt}) \quad (3)$$

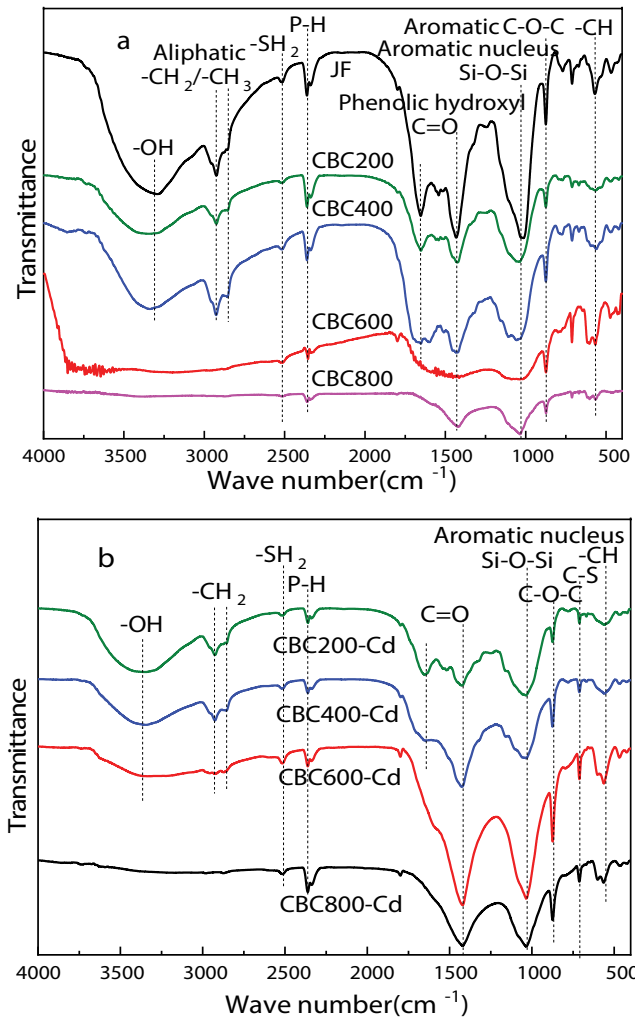


Fig. 2. Fourier-transform infrared (FTIR) spectra of CBCs (a) before and (b) after the Cd(II) adsorption.

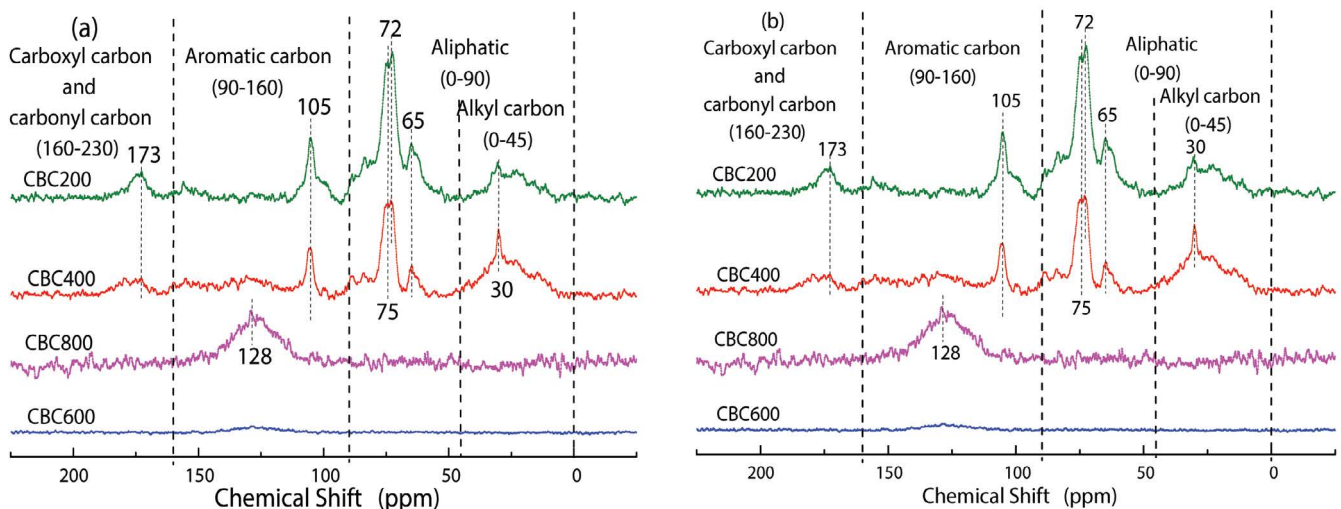


Fig. 3. Cross-polarization-magic angle spinning ^{13}C nuclear magnetic resonance spectrograms of CBCs (a) before and (b) after the Cd(II) adsorption.

where Q_t (mg g^{-1}) and Q_e (mg g^{-1}) are the Cd(II) sorption capacities at time t and equilibrium, respectively. t (min) is the adsorption time, and K (min^{-1}) is the adsorption rate constant of the pseudo-first-order model.

The pseudo-second-order model equation is as follows:

$$Q_t = \frac{Q_e^2 K_1 t}{1 + Q_e K_1 t} \quad (4)$$

where Q_t (mg g^{-1}), Q_e (mg g^{-1}), and t (min) is the adsorption time, and K_1 ($\text{mg g}^{-1} \text{min}^{-1}$) is the adsorption rate constant of the pseudo-second-order model.

The effect of different contact times on Cd(II) adsorption by CBCs pyrolyzed at different temperatures is shown in Fig. 5a. Adsorption studies of CBCs' removal of Cd(II) were conducted for 1,440 min to evaluate the adsorption kinetics; adsorption equilibrium was achieved in approximately 720–1,440 min. The Cd(II) equilibrium pH and adsorption capacities increased drastically in the first 60 min for CBCs formed at all pyrolysis temperatures. This could arise from the rapid occupation of easily accessible external surface adsorption sites on the CBCs, and mechanisms such as outer-sphere complexation [26]. There have also been studies that the rapid adsorption equilibrium suggests that electrostatic adsorption may promote the adsorption of Cd(II) to organic components of biochar [27,28]. The increases in adsorption capacity achieved equilibrium after 120 min. In the late stages, this slow equilibrium may be related to the formation of inner-layer complexes, or to the saturation of adsorption sites, and the physical or chemical characteristics of the CBCs [29]. The CBC600 exhibited the highest adsorption efficiency, equilibrium pH, and capacity for Cd(II). The adsorption capacities were 45.50, 49.17, 52.02, and 49.34 mg g^{-1} for CBC200, CBC400, CBC600, and CBC800, respectively (Table 1), and the corresponding equilibrium pH values were 6.57, 6.64, 8.41, and 7.92, respectively. The Cd(II) removal rates were 78.70%, 78.76%, 79.72%, and 78.92%, respectively. Compared with other

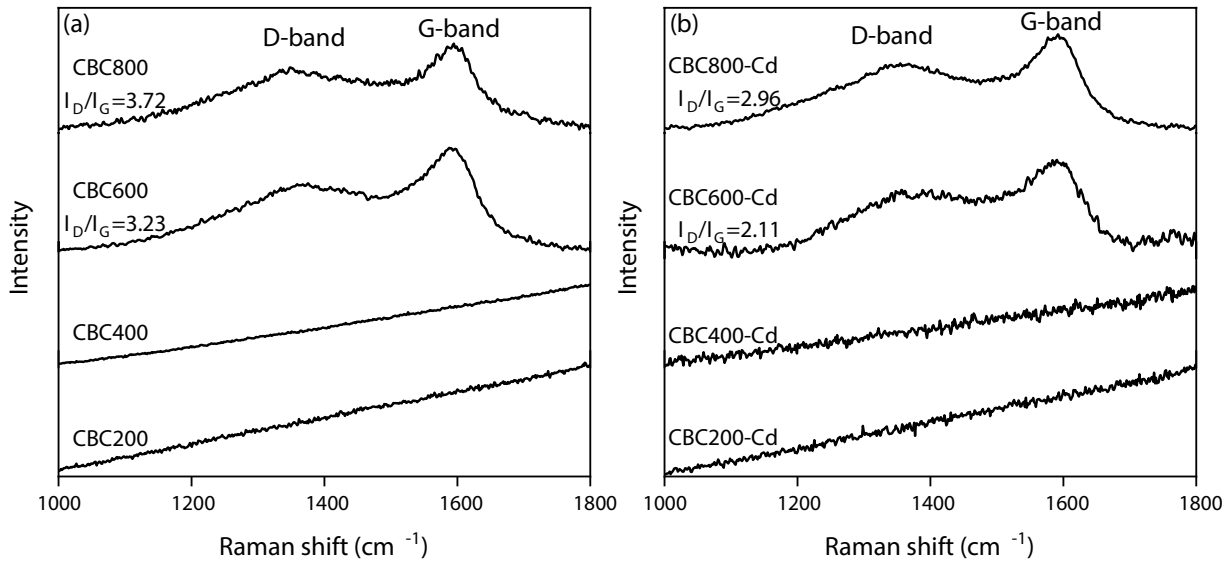


Fig. 4. Raman spectra of CBCs (a) before and (b) after the Cd(II) adsorption.

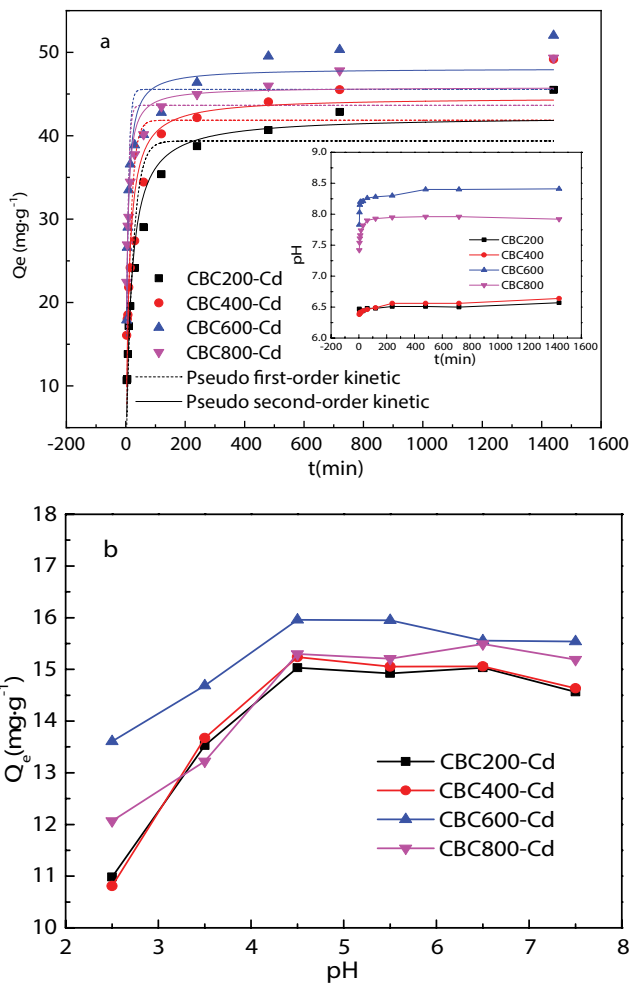


Fig. 5. Adsorption kinetics of Cd(II) on CBC200, CBC400, CBC600, and CBC800. Effect of initial solution pH on Cd(II) adsorption by CBC200, CBC400, CBC600, and CBC800.

biochar derived from manure, the maximum adsorption capacity of CBC was highest among the related materials (Table 2). The partition coefficient (P_c) is an important parameter reflecting the adsorption capacity of the adsorbent [39]. The CBC200, CBC400, CBC600, and CBC800 exhibited a P_c of 11.26, 14.75, 18.25 and 15.18 $\text{mg g}^{-1} \mu\text{M}^{-1}$, respectively. The results proved CBCs to be a potent adsorption material. As the pyrolysis temperatures were increased, the removal rates increased, suggesting that higher-temperature pyrolysis enhances the removal efficiency of Cd(II) by CBC. Simultaneously, the increase may be because of the higher surface areas, stronger affinities, greater porosities, more numerous adsorption sites, and larger amounts of carbonate minerals and precipitates [11].

The pseudo-second-order model (with R^2 values of 0.96, 0.91, 0.94, and 0.93 for CBC200, CBC400, CBC600, and CBC800, respectively) is a better fit for the kinetics of Cd(II) sorption than the pseudo-first-order model (which has R^2 values of 0.8755, 0.7814, 0.8329, and 0.7638 for CBC200, CBC400, CBC600, and CBC800, respectively), as shown in Table 1. R^2 values are >0.9 for all CBCs in the pseudo-second-order model. This indicates that the rate-limiting step in Cd(II) adsorption by CBC is a chemical adsorption process. This process may comprise the sharing or exchange of electrons between Cd(II) and the CBC as covalent bonds [40].

3.3. Isotherm of Cd adsorption

The isothermal adsorption of Cd(II) from aqueous solutions of 0–200 mg L^{-1} onto CBCs was studied at solution temperatures of 288, 298, and 308 K, as illustrated in Fig. 6. To further explain the adsorption performances and mechanisms of Cd(II) on CBC surfaces, the adsorption isotherm data were fitted by the Langmuir and Freundlich models. The Langmuir model is as follows:

$$\frac{Q_e}{Q_{\max}} = \frac{bC_e}{1 + bC_e} \quad (5)$$

Table 1
Parameters of pseudo-first-order and pseudo-second-order kinetic models for Cd(II) adsorption by CBCs

Adsorbent	Pseudo-first-order model				Pseudo-second-order model		
	Q_A^a (mg g ⁻¹)	Q_e^b (mg g ⁻¹)	K^c (g mg ⁻¹ min ⁻¹)	R^2	Q_e (mg g ⁻¹)	K_1^d (g mg ⁻¹ min ⁻¹)	R^2
CBC200	45.50	39.37	0.04	0.88	42.33	0.0014	0.96
CBC400	49.17	41.86	0.07	0.78	44.60	0.0021	0.91
CBC600	52.02	45.55	0.14	0.83	48.07	0.0044	0.94
CBC800	49.34	43.65	0.16	0.76	45.82	0.0054	0.93

Note: a : Q_A represented the amount of Cd(II) adsorbed by CBC at actual equilibrium. b : Q_e represented the amount of Cd(II) adsorbed by CBC at equilibrium. c : K and K_1 represented the rate constants of pseudo-first-order and pseudo-second-order adsorption, respectively.

Table 2
Maximum adsorption capacities for Cd(II) onto related materials reported in the literature

Adsorbents	Q_{\max} (mg g ⁻¹)	References
Chicken manure biochar	50.46	This work
Poultry litter biochar	4.62	[30]
Cattle manure biochar	4.00	[31]
Dairy manure biochar	23.64	[32]
Cattle manure biochar	14.71	
Swine manure biochar	0.73	[33]
Poultry manure biochar	5.13	
Swine manure biochar	46.5	[34]
Chicken litter biochar	48.5	[35]
Poultry litter biochar	24.53	[36]
Swine manure biochar	22.68	[37]
Dairy manure biochar	31.92	[38]

where b (L mg⁻¹) is the Langmuir adsorption equilibrium constant; Q_{\max} (mg g⁻¹) is the maximum adsorption capacity, and Q_e (mg g⁻¹) and C_e (mg g⁻¹) have the same definitions as given in Eq. (5).

The Freundlich model is as follows:

$$Q_e = K_f \cdot C_e^{\frac{1}{n}} \quad (6)$$

where K_f (mg g⁻¹ (mg L⁻¹) ^{n}) is the Freundlich adsorption equilibrium constant and $1/n$ is the adsorption affinity.

The adsorption rates gradually slowed down until adsorption equilibrium with increasing adsorption temperature, initial concentration, and pyrolysis temperature which resulted from that low initial solution concentration of the Cd(II) usually accompanied with rapid adsorption rates since there were abundant adsorption sites on materials surfaces. However, the adsorption sites were gradually occupied until all sites are saturated as the initial concentration of Cd(II) increase [41]. The Cd(II) adsorption capacities are maximized at a solution temperature of 308 K. The Cd(II) adsorption capacities followed the order CBC600 > CBC800 > CBC400 > CBC200 at all solution temperatures. These results show that higher solution temperatures enhance the endothermal adsorption characteristics. In addition,

they confirm the strong adsorption affinity of CBC600. This result may arise from the morphological characteristics and functional group contents in these four CBCs [42].

The adsorption isotherms of Cd(II) onto CBCs prepared at four pyrolysis temperatures were further fitted with the Langmuir and Freundlich models, with results as presented in Table 3. The R^2 of the Langmuir model (0.98) was higher than that of the Freundlich model (0.93) for all solution temperatures. Accordingly, the Langmuir model is better fitted for the entire range of adsorption isotherms.

3.4. Adsorption mechanism of Cd onto CBC

The SEM images of the CBCs after Cd(II) adsorption are shown in Figs. 1e–h. After Cd(II) adsorption, the surface morphology of CBCs displayed rougher and particulate matter was attached to the surface of CBCs. The TEM images of CBCs after adsorption (Figs. 1E–H) shown particle agglomerates within CBCs. The results of SEM-TEM images suggested that physical pore filling is one of the mechanisms responsible for Cd(II) removal [14].

As shown in Fig. 2b, the FTIR spectra of CBCs after the adsorption of Cd(II) showed that the intensity of absorption peaks at 3,310 cm⁻¹ decreased. The changes may correspond to the surface complexation of Cd(II) with the hydroxyl (–OH) and carboxylic (–COOH) functional groups in CBC [43]. The carbonyl oxygen ions on the biochars' surface serve as an electron donor. The vibration intensity of the C=O stretching peak decreased and a shift to lower wavenumber was found, suggested the carboxyl could complex with Cd(II) through monodentate and bidentate bridging [41]. The absorption peaks at 547 and 708 cm⁻¹ may arise from the different stretching vibrational modes and symmetric bending modes of phosphate (PO₄³⁻) groups [44], which were significant in the adsorption of Cd(II). The region between 1,056 and 1,014 cm⁻¹ represents the Si–O–Si stretching vibration. The intensity of the absorption peaks had a great chance for was greatest at carbonization temperature of CBC200, CBC400, CBC600 and CBC600 after treatment with Cd. Due to the richness of electron-donating functional groups such as oxygenic functional groups (–OH, –COO–, etc.) and aromatic rings in CBC, it be involved in complexation with Cd(II) through C– π interaction [45].

In order to elucidate the role of CBCs adsorption material in the adsorption mechanism during the adsorption of Cd(II), further characterization by solid-state CP-MAS ¹³C-NMR and Raman spectra was performed. The peaks

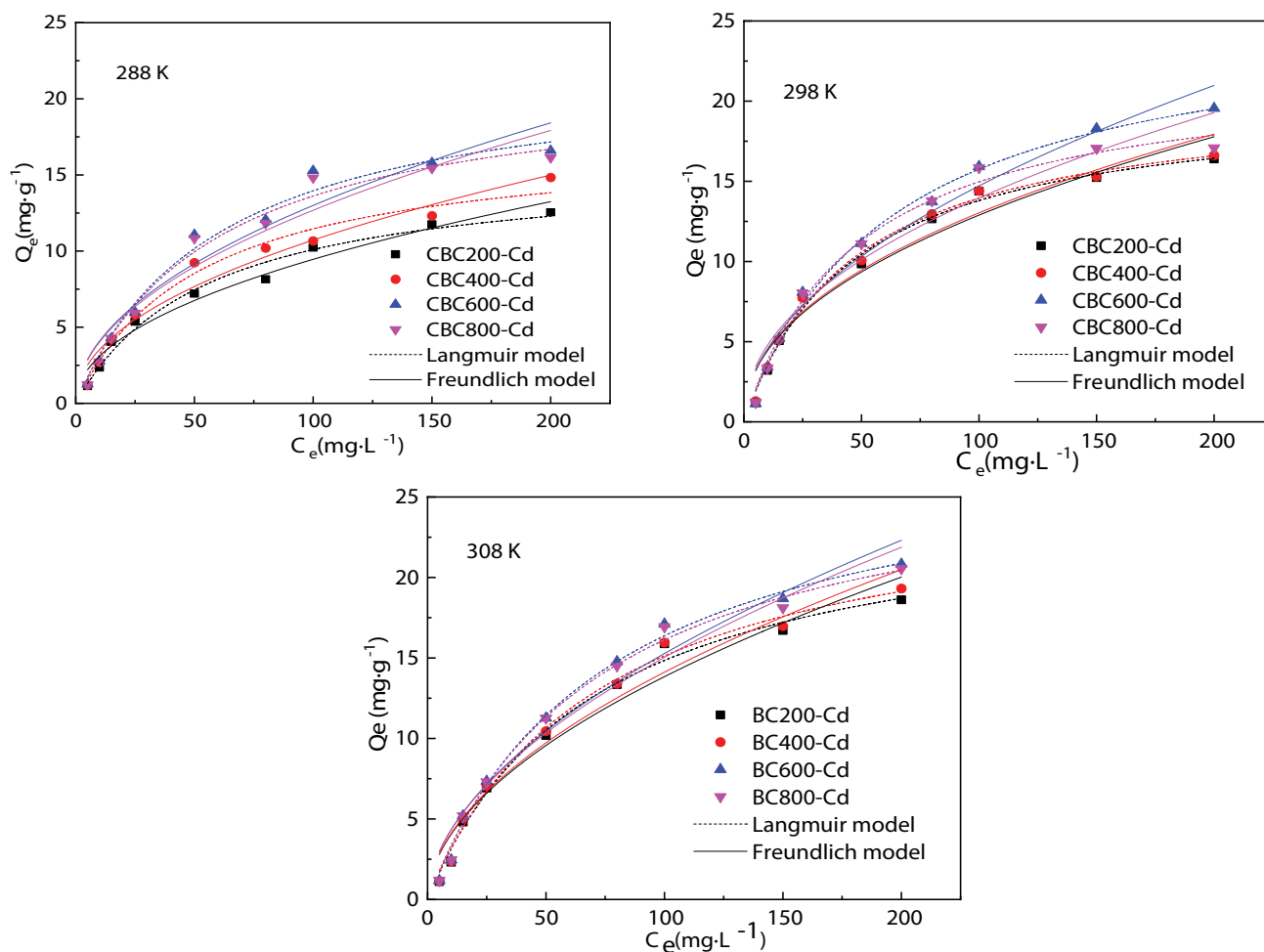


Fig. 6. Adsorption isotherms of Cd(II) on CBC200, CBC400, CBC600, and CBC800.
Note: 288, 298 and 308 K in the image labels indicate the CBC adsorption temperatures.

showed a weak distribution of carboxyl and carbonyl carbons between 160 and 230 ppm, the individual peaks showed a decrease after the Cd(II) adsorption. The CP-MAS ^{13}C -NMR peaks of pre-adsorption CBC800 were mainly distributed in the aromatic carbon region of 90–160 ppm. these peaks decrease after the Cd(II) adsorption, indicating that the combination of Cd and BC through C- π interactions [46]. A significant decrease in the intensity of D and G bands after Cd(II) adsorption by CBC600 and CBC800, suggesting that a strong charge transfer from Cd(II) to the biochar during the adsorption [40]. Meanwhile, the I_D/I_G of CBC600 and CBC800 decreased by 0.92 and 0.76, respectively, identifying the existence of C- π interaction [47].

Based on the results upon, the dominant adsorption mechanisms are prosed in Fig. 7, mainly including pore filling, complexation and precipitation, and Cp-cation interaction [48]:

- *Pore filling*: SEM-TEM indicated the Cd ions could be fill in the pore of CBC.
- *Complexation*: CBC had the richness of electron-donating functional groups such as oxygenic functional groups

(-OH, -COO-, etc.) and aromatic rings, it can bind with Cd(II).

- *C- π interaction*: FTIR, ^{13}C -NMR and Raman spectra analysis indicated that aromatic structure of CBC played an important role in the removal of Cd through the interaction of π - π .
- *Precipitation*: according to SEM-TEM, FTIR and ^{13}C -NMR characterization, the aliphatic compounds (alkyl carbon), carbohydrates (methoxy carbon, hydroxyl carbon), carboxyl carbons, and carbonyl carbons in CBC will precipitate with Cd(II).

4. Conclusions

The properties of the CBC were significantly affected by pyrolysis temperature. The sorption capacities of Cd by CBC were enhanced with the increasing of pyrolytic temperature. The kinetics of Cd(II) adsorption onto the CBCs followed the pseudo-second-order kinetics model, and the adsorption isotherm study showed that the equilibrium results of Cd(II) adsorption onto the CBCs fit the Langmuir model. The initial pH most conducive to the adsorption

Table 3
Parameters of Langmuir and Freundlich models for Cd(II) adsorption by CBCs

T (K)	Langmuir model				Freundlich model		
	Adsorbent	Q_m^a (mg g ⁻¹)	b^b (L mg ⁻¹)	R^2	K_f^b (mg g ⁻¹)	n^c	R^2
288	CBC200	15.68	0.0181	0.98	1.01	0.49	0.97
	CBC400	17.44	0.0192	0.98	1.16	0.48	0.96
	CBC600	22.29	0.0168	0.98	1.28	0.50	0.93
	CBC800	21.57	0.0171	0.98	1.27	0.50	0.93
298	CBC200	20.31	0.0212	0.99	1.52	0.46	0.94
	CBC400	50.46	0.0214	0.99	1.56	0.46	0.95
	CBC600	25.65	0.0159	0.99	1.39	0.51	0.97
	CBC800	22.18	0.0208	0.99	1.66	0.47	0.93
308	CBC200	25.29	0.0142	0.99	1.19	0.53	0.95
	CBC400	26.04	0.0139	0.99	1.19	0.54	0.96
	CBC600	28.79	0.0132	0.99	1.23	0.55	0.96
	CBC800	27.93	0.0137	0.99	1.25	0.54	0.96

Note: a: Q_m represented maximum adsorption capacity. a: b and K_f represented adsorption equilibrium constants of Langmuir and Freundlich models, respectively. c: $1/n$ represented the adsorption affinity.

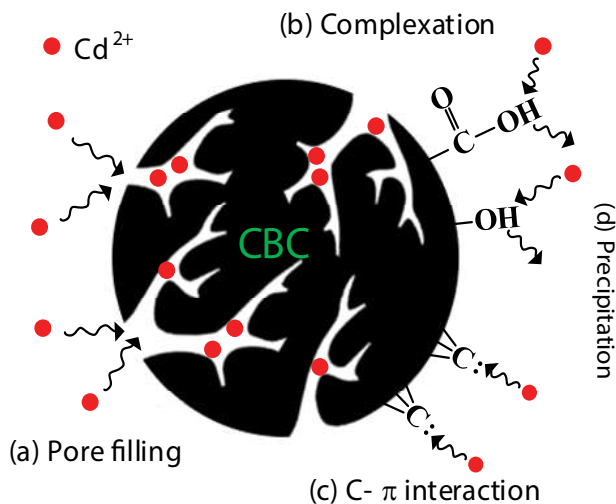


Fig. 7. Proposed mechanism for removal of Cd(II) from aqueous solution by CBC.

of Cd(II) was 4.5. The adsorption capacity of Cd was in the order of CBC600 > CBC800 > CBC400 > CBC200, and the maximum Cd adsorption capacities reached 52.02 mg g⁻¹. Based on the analysis of SEM-TEM, FTIR, ¹³C-NMR and Raman, the dominant adsorption mechanisms of Cd on CBC involved pore filling, complexation, precipitation and C- π interaction.

Acknowledgment

This work was supported by the National Key Research and Development Program of China (2017YFD0801402; 2018YFD0800300), National Natural Science Foundation

of China (31971525), and the Central Public-Scientific Institution Basal Research Fund (Y2020PT03).

References

- [1] X.Y. Zeng, D.S. Zou, A.D. Wang, Y.Y. Zhou, Y.H. Liu, Z.H. Li, F. Liu, H. Wang, Q.R. Zeng, Z.H. Xiao, Remediation of cadmium-contaminated soils using *Brassica napus*: effect of nitrogen fertilizers, *J. Environ. Manage.*, 255 (2020) 109885, doi: 10.1016/j.jenvman.2019.109885.
- [2] R.-Z. Wang, D.-L. Huang, Y.-G. Liu, C. Zhang, C. Lai, G.-M. Zeng, M. Cheng, X.-M. Gong, J. Wan, H. Luo, Investigating the adsorption behavior and the relative distribution of Cd²⁺ sorption mechanisms on biochars by different feedstock, *Bioresour. Technol.*, 261 (2018) 265–271.
- [3] I.M. Lima, K.S. Ro, G.B. Reddy, D.L. Boykin, K.T. Klasson, Efficacy of chicken litter and wood biochars and their activated counterparts in heavy metal clean up from wastewater, *Agriculture*, 5 (2015) 806–825.
- [4] S.H. Li, D.S. Zou, L.C. Li, L. Wu, F. Liu, X.Y. Zeng, H. Wang, Y.F. Zhu, Z.H. Xiao, Evolution of heavy metals during thermal treatment of manure: a critical review and outlooks, *Chemosphere*, 247 (2020) 125962, doi: 10.1016/j.chemosphere.2020.125962.
- [5] A.G. Caporale, M. Pigna, A. Sommella, P. Conte, Effect of pruning-derived biochar on heavy metals removal and water dynamics, *Biol. Fertil. Soils*, 50 (2014) 1211–1222.
- [6] R. Goswami, J.H. Shim, S. Deka, D. Kumari, R. Katak, M. Kumar, Characterization of cadmium removal from aqueous solution by biochar produced from *Ipomoea fistulosa* at different pyrolytic temperatures, *Ecol. Eng.*, 97 (2016) 444–451.
- [7] L. Beesley, M. Marmiroli, The immobilisation and retention of soluble arsenic, cadmium and zinc by biochar, *Environ. Pollut.*, 159 (2011) 474–480.
- [8] F.S. Higashikawa, R.F. Conz, M. Colzato, C.E.P. Cerri, L.R.F. Alleoni, Effects of feedstock type and slow pyrolysis temperature in the production of biochars on the removal of cadmium and nickel from water, *J. Cleaner Prod.*, 137 (2016) 965–972.
- [9] K.L. Qiao, W.J. Tian, J. Bai, J. Dong, J. Zhao, X.X. Gong, S.H. Liu, Preparation of biochar from enteromorpha prolifera and its use for the removal of polycyclic aromatic hydrocarbons (PAHs) from aqueous solution, *Ecotoxicol. Environ. Saf.*, 149 (2018) 80–87.

- [10] Z. Zhou, Z.H. Xu, Q.J. Feng, D.H. Yao, J.G. Yu, D.S. Wang, S.Q. Lv, Y.F. Liu, N. Zhou, M.-E. Zhong, Effect of pyrolysis condition on the adsorption mechanism of lead, cadmium and copper on tobacco stem biochar, *J. Cleaner Prod.*, 187 (2018) 996–1005.
- [11] J. Jiang, R.-K. Xu, Application of crop straw derived biochars to Cu(II) contaminated Ultisol: evaluating role of alkali and organic functional groups in Cu(II) immobilization, *Bioresour. Technol.*, 133 (2013) 537–545.
- [12] Z. Chen, T. Liu, J.J. Tang, Z.J. Zheng, H.M. Wang, Q. Shao, G.L. Chen, Z.X. Li, Y.Q. Chen, J.W. Zhu, T. Feng, Characteristics and mechanisms of cadmium adsorption from aqueous solution using lotus seedpod-derived biochar at two pyrolytic temperatures, *Environ. Sci. Pollut. Res.*, 25 (2018) 11854–11866.
- [13] D. Cholico-González, N. Ortiz Lara, A.M.F. Macedo, J.C. Salas, Adsorption behavior of Pb(II), Cd(II), and Zn(II) onto agave bagasse, characterization, and mechanism, *ACS Omega*, 5 (2020) 3302–3314.
- [14] C.X. Yan, Y.M. Xu, L. Wang, X.F. Liang, Y.B. Sun, H.T. Jia, Effect of different pyrolysis temperatures on physico-chemical characteristics and lead(II) removal of biochar derived from chicken manure, *RSC Adv.*, 10 (2020) 3667–3674.
- [15] S. Álvarez-Torrellas, A. Rodríguez, G. Ovejero, J. García, Comparative adsorption performance of ibuprofen and tetracycline from aqueous solution by carbonaceous materials, *Chem. Eng. J.*, 283 (2016) 936–947.
- [16] M.T. Sekulić, S. Pap, Z. Stojanović, N. Bošković, J. Radonić, T.Š. Knudsen, Efficient removal of priority, hazardous priority and emerging pollutants with *Prunus armeniaca* functionalized biochar from aqueous wastes: experimental optimization and modeling, *Sci. Total Environ.*, 613–614 (2018) 736–750.
- [17] Z.T. Shen, Y.H. Zhang, F. Jin, D.S. Alessi, Y.Y. Zhang, F. Wang, O. McMillan, A. Al-Tabbaa, Comparison of nickel adsorption on biochars produced from mixed softwood and *Miscanthus* straw, *Environ. Sci. Pollut. Res.*, 25 (2018) 1–10.
- [18] H. Wikberg, S.L. Maunu, Characterisation of thermally modified hard- and softwoods by CP-MAS ¹³C NMR, *Carbohydr. Polym.*, 58 (2004) 461–466.
- [19] R. El Hage, N. Brosse, L. Chrusciel, C. Sanchez, P. Sannigrahi, A. Ragauskas, Characterization of milled wood lignin and ethanol organosolv lignin from *Miscanthus*, *Polym. Degrad. Stab.*, 94 (2009) 1632–1638.
- [20] E. Tronc, C.A. Hernández-Escobar, R. Ibarra-Gómez, A. Estrada-Monje, J. Navarrete-Bolaños, E.A. Zaragoza-Contreras, Blue agave fiber esterification for the reinforcement of thermoplastic composites, *Carbohydr. Polym.*, 67 (2007) 245–255.
- [21] S.Y. Wei, Influence of Biomass Feedstocks and Pyrolysis Temperatures on Physical and Chemical Properties of Biochar, Graduate University of Chinese Academy of Sciences (Guangzhou Institute of Geochemistry, Chinese Academy of Sciences), 2017.
- [22] M. Nahata, C.Y. Seo, P. Krishnakumar, J. Schwank, New approaches to water purification for resource-constrained settings: production of activated biochar by chemical activation with diammonium hydrogenphosphate, *Front. Chem. Sci. Eng.*, 12 (2018) 194–208.
- [23] O. Paris, C. Zollfrank, G.A. Zickler, Decomposition and carbonisation of wood biopolymers—a microstructural study of softwood pyrolysis, *Carbon*, 43 (2005) 53–66.
- [24] P. Singh, R. Singh, V.K. Singh, A. Borthakur, S. Madhav, V.K. Singh, D. Tiwary, V.C. Srivastava, P.K. Mishra, Exploring temple floral refuse for biochar production as a closed loop perspective for environmental management, *Waste Manage.*, 77 (2018) 78–86.
- [25] H. Gogoi, T. Leiviskä, J. Rämö, J. Tanskanen, Production of aminated peat from branched polyethylenimine and glycidyltrimethylammonium chloride for sulphate removal from mining water, *Environ. Res.*, 175 (2019) 323–334.
- [26] G. Bin, X.D. Cao, Y. Dong, Y.M. Luo, L.Q. Ma, Colloid deposition and release in soils and their association with heavy metals, *Crit. Rev. Env. Sci. Technol.*, 41 (2011) 336–372.
- [27] W.H. Zhang, I.M. Lo, EDTA-enhanced washing for remediation of Pb- and/or Zn-contaminated soils, *J. Environ. Manage.*, 132 (2006) 1282–1288.
- [28] X.Y. Xu, X.D. Cao, L. Zhao, H.J. Zhou, Q.S. Luo, Interaction of organic and inorganic fractions of biochar with Pb(II) ion: further elucidation of mechanisms for Pb(II) removal by biochar, *RSC Adv.*, 4 (2014) 44930–44937.
- [29] Z. Zhou, Y.-G. Liu, S.-B. Liu, H.-Y. Liu, G.-M. Zeng, X.-F. Tan, C.-P. Yang, Y. Ding, Z.-L. Yan, X.-X. Cai, Sorption performance and mechanisms of arsenic(V) removal by magnetic gelatin-modified biochar, *Chem. Eng. J.*, 314 (2017) 223–231.
- [30] T. Bandara, J.M. Xu, I.D. Potter, A. Franks, J.B.A.J. Chathurika, C.X. Tang, Mechanisms for the removal of Cd(II) and Cu(II) from aqueous solution and mine water by biochars derived from agricultural wastes, *Chemosphere*, 254 (2020) 126745, doi: 10.1016/j.chemosphere.2020.126745.
- [31] S.Y. Wang, J.-H. Kwak, M.S. Islam, M.A. Naeth, M.G. El-Din, S.X. Chang, Biochar surface complexation and Ni(II), Cu(II), and Cd(II) adsorption in aqueous solutions depend on feedstock type, *Sci. Total Environ.*, 712 (2020) 136538, doi: 10.1016/j.scitotenv.2020.136538.
- [32] Z.-I. Chen, J.-q. Zhang, L. Huang, Z.-h. Yuan, Z.-j. Li, M.-c. Liu, Removal of Cd and Pb with biochar made from dairy manure at low temperature, *J. Integr. Agric.*, 18 (2019) 201–210.
- [33] S.C. Lei, Y. Shi, Y.P. Qiu, L. Che, C. Xue, Performance and mechanisms of emerging animal-derived biochars for immobilization of heavy metals, *Sci. Total Environ.*, 646 (2019) 1281–1289.
- [34] Y.Y. Deng, S. Huang, D.A. Laird, X.G. Wang, C.Q. Dong, Quantitative mechanisms of cadmium adsorption on rice straw- and swine manure-derived biochars, *Environ. Sci. Pollut. Res.*, 25 (2018) 32418–32432.
- [35] F.J. Qi, Y.B. Yan, D. Lamb, R. Naidu, N.S. Bolan, Y.J. Liu, Y.S. Ok, S.W. Donne, K.T. Semple, Thermal stability of biochar and its effects on cadmium sorption capacity, *Bioresour. Technol.*, 246 (2017) 48–56.
- [36] L.F. Han, H.R. Sun, K.S. Ro, K. Sun, J.A. Libra, B.S. Xing, Removal of antimony(III) and cadmium(II) from aqueous solution using animal manure-derived hydrochars and pyrochars, *Bioresour. Technol.*, 234 (2017) 77–85.
- [37] D.Y. Xu, Y. Zhao, K. Sun, B. Gao, Z.Y. Wang, J. Jin, Z.Y. Zhang, S.F. Wang, Y. Yan, X.T. Liu, F.C. Wu, Cadmium adsorption on plant- and manure-derived biochar and biochar-amended sandy soils: impact of bulk and surface properties, *Chemosphere*, 111 (2014) 320–326.
- [38] X.Y. Xu, X.D. Cao, L. Zhao, H.L. Wang, H.R. Yu, B. Gao, Removal of Cu, Zn, and Cd from aqueous solutions by the dairy manure-derived biochar, *Environ. Sci. Pollut. Res.*, 20 (2013) 358–368.
- [39] S. Batool, M. Idrees, M. Ahmad, M. Ahmad, Q. Hussain, A. Iqbal, J. Kong, Design and characterization of a biomass template/SnO₂ nanocomposite for enhanced adsorption of 2,4-dichlorophenol, *Environ. Res.*, 181 (2019) 108955, doi: 10.1016/j.envres.2019.108955.
- [40] K.J. Sun, J.C. Tang, Y.Y. Gong, H.R. Zhang, Characterization of potassium hydroxide (KOH) modified hydrochars from different feedstocks for enhanced removal of heavy metals from water, *Environ. Sci. Pollut. Res.*, 22 (2015) 16640–16651.
- [41] J.Q. Deng, X.D. Li, Y.G. Liu, G.M. Zeng, J. Liang, B. Song, X. Wei, Alginate-modified biochar derived from Ca(II)-impregnated biomass: excellent anti-interference ability for Pb(II) removal, *Ecotoxicol. Environ. Saf.*, 165 (2018) 211–218.
- [42] F. Yang, Y. Gao, L.L. Sun, S.S. Zhang, J.J. Li, Y. Zhang, Effective sorption of atrazine by biochar colloids and residues derived from different pyrolysis temperatures, *Environ. Sci. Pollut. Res.*, 25 (2018) 18528–18539.
- [43] M.A. Wahab, S. Jellali, N. Jedidi, Ammonium biosorption onto sawdust: FTIR analysis, kinetics and adsorption isotherms modeling, *Bioresour. Technol.*, 101 (2010) 5070–5075.
- [44] P. Stoch, A. Stoch, M. Ciecinska, I. Krakowiak, M. Sitarz, Structure of phosphate and iron-phosphate glasses by DFT

- calculations and FTIR/Raman spectroscopy, *J. Non-Cryst. Solids*, 450 (2016) 48–60.
- [45] Y.L. Mei, B. Li, S.S. Fan, Biochar from rice straw for Cu^{2+} removal from aqueous solutions: mechanism and contribution made by acid-soluble minerals, *Water Air Soil Pollut.*, 231 (2020) 420, <https://doi.org/10.1007/s11270-020-04791-9>.
- [46] C. De Pasquale, V. Marsala, A.E. Berns, M. Valagussa, A. Pozzi, G. Alonzo, P. Conte, Fast field cycling NMR relaxometry characterization of biochars obtained from an industrial thermochemical process, *J. Soils Sediments*, 12 (2012) 1211–1221.
- [47] J. Mcdonald-Wharry, M. Manley-Harris, K. Pickering, Carbonisation of biomass-derived chars and the thermal reduction of a graphene oxide sample studied using Raman spectroscopy, *Carbon*, 59 (2013) 383–405.
- [48] M. Li, Y.Y. Tang, N. Ren, Z.T. Zhang, Y.M. Cao, Data processing to support explication about effect of mineral constituents on temperature-dependent structural characterization of carbon fractions in sewage sludge-derived biochar, *Data Brief*, 17 (2018) 1304–1306.